

lar Ca^{2+} concentrations, therefore, the induced calcium homeostasis leads to the activation of many calcium-sensitive proteins implicated in AD [11, 12]. The $A\beta$ peptides are derived from enzymatic cleavage of type I transmembrane amyloid precursor protein (APP) with about 39–43 residues long. There are two important variants of $A\beta$ peptide in human: $A\beta_{1-40}$ and $A\beta_{1-42}$, of which the latter could form fibrils much more rapidly [13]. There is also a conclusive evidence showing that $A\beta_{1-42}$ could rapidly form hexamers and dodecamers with the dodecamers seeding the formation of extended preprotofibrils by using high resolution atomic force microscopy [14, 15].

$A\beta_{25-35}$ has been known as the shortest active fragment that tends to form large β -sheet aggregated structures from a soluble random coil form and remains toxic as $A\beta_{1-42}$ [16, 17], and also has been often chosen as a model for full length $A\beta$ in structural and functional studies because of its conformational transition dynamic feature which has been revealed with the help of 2D NMR, CD and FTIR spectroscopy [18–20].

Inhibition of aggregation of oligomers is known to be one of principal strategies for the development of treatment for AD. In the early stage of AD, not only the accumulation of $A\beta$ peptides in neuritic plaques is important, but also the diminished nicotinic transmission can not be ignored since the reduced acetylcholine (ACh) levels and declines of the numbers of nicotinic acetylcholine receptors (nAChR) in affected tissues [21]. The $\alpha 7$ -nAChR is one of the mostly expressed nicotinic receptors, which has high permeability to calcium, and the onset of AD is known to be correlated with the malfunction of $\alpha 7$ -nAChR [22]. The $\alpha 7$ -nAChR is a homopentameric ligand-gated ion channel with unique pharmacological and physiological properties and it exhibits an exceptionally high $A\beta$ affinity. Therefore, the aberrant accumulation of misfolded $A\beta$ peptide would trigger the synaptic and neural network dysfunction [23]. Deleting the $\alpha 7$ -nAChR gene leads to impairment of memory and cognition, thus $\alpha 7$ -nAChR is a therapeutic target for AD [24].

In order to prevent the onset of AD, it would be important to develop a drug that has potential ability to modulate nAChR and prevent the accumulation of $A\beta$ in the receptor's ion channel. Although there are existing drugs, such as galantamine, GTS-21, AQW051, donepezil, have been reported to provide disease-modifying effect and significantly reduce the $A\beta$ level in brain [25–27], they have mainly taken effect during the early stage of AD. Future drug developments will depend on providing new drugs and revealing possible mechanisms involved in AD. For a better understanding about the intermolecular interactions between $A\beta$ and $\alpha 7$ -nAChR, the possible non-bonded interactions within $A\beta$ and receptor need to be revealed, and a reasonable treatment for breaking their abnormal binding should be developed.

Revealing the interactions between $A\beta$ fragments and

receptor, not only the structural tools with spatial resolution at molecular level should be employed for the prediction of 3D structure of $A\beta$ monomer or oligomer [8, 13, 28], but also the experimental equipments with ultrafast time resolution would be necessary for the understanding about the aggregation dynamics and the structural fluctuation during the binding process of $A\beta$ and receptor [29, 30].

Recently developed two dimensional infrared spectroscopy (2D IR) has been known as a powerful tool for extracting structural and dynamic information from biological and materials science [31]. The main advantages of 2D IR are its structural sensitivity and ultrafast time resolution, 2D IR can decipher the specific folding states and their transition pathways of special amino acid residues that encoded in the backbone amide vibrational parameters at femtosecond to picosecond time resolution [31–33]. DFT (density functional theory) calculations, molecular dynamics simulations and spectral modeling were widely used for the prediction of structural dynamics of polypeptides that encoded in the vibrational signals, and for revealing the correlations among molecular structure, vibrational parameters, and surrounding chemical environments [34]. Thus, the understanding of conformational characters of polypeptides and their structural dynamics of state-to-state transitions can be achieved [35–42].

In the present work, semi-flexible docking was employed for the demonstration of the interactions between $A\beta_{25-35}$ fragment and $\alpha 7$ -nAChR. The structural dynamics of the docked complex of $A\beta_{25-35}/\alpha 7$ -nAChR in aqueous solution were evaluated, and statistic analysis was performed for the most probable configurations of $A\beta_{25-35}$. Amide-I vibrations which have been proven to be sensitive to the peptide's secondary structure, were examined for the understanding of the dynamical structure of $A\beta_{25-35}$ and its possible aggregation process within the complex. Virtual screening was carried out for the existing drugs (lead compounds) that can dock to the active sites of $\alpha 7$ -nAChR, then the pharmacophore simulation and semi-flexible docking were performed for the design and evaluation of new drugs.

II. COMPUTATIONAL METHODS

A. Molecular docking

The pdb files of $A\beta_{25-35}$ (PDB ID:1QXC, FIG. 1(A)) and $\alpha 7$ -nAChR (PDB ID:3SQ6, FIG. 1(B)) were downloaded from RCSB database. $\alpha 7$ -nAChR is a homopentameric ligand-gated ion channel, and it is consist of five identical polypeptide chain that denoted as A, B, C, D, and E. $A\beta_{25-35}$ was solvated in a cubic box with its side length of 54 Å for molecular dynamics simulations (simulation details were the same as stated in Section II B). The most probable conformation of $A\beta_{25-35}$ obtained from MD simulation was used for the molecular

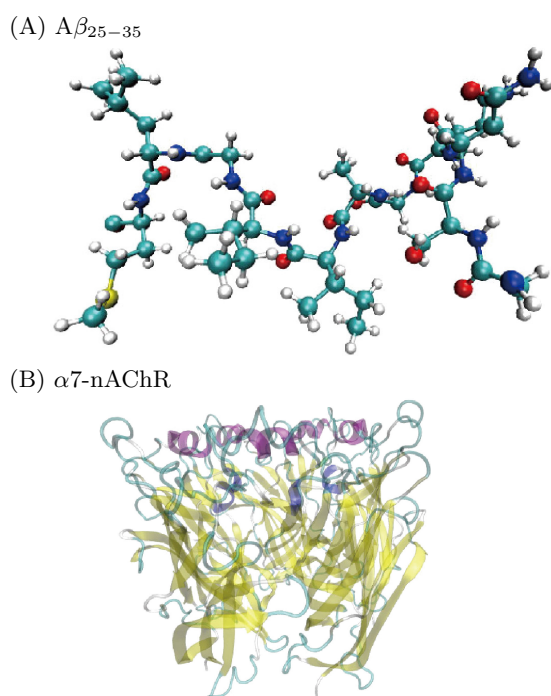


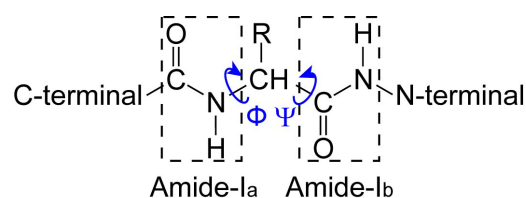
FIG. 1 The molecular structures of $A\beta_{25-35}$ fragment (A) and $\alpha 7$ -nAChR (B). For color image, see the online version.

docking. The semi-flexible docking method was carried out to obtain the docking poses by using the ligfit module in Discovery Studio 2.5. Scoring functions (PLP1 and PLP2) were employed for the evaluation about the efficiency and reliability of the docking results.

B. Molecular dynamics simulations

All atom molecular dynamics simulations were performed for $A\beta_{25-35}/\alpha 7$ -nAChR complex in aqueous solution by using NAMD package [43]. The most preferred docking pose of the complex was used for the initial configuration. The complex was solvated in a box with its side length of $112 \text{ \AA} \times 107 \text{ \AA} \times 109 \text{ \AA}$ filled with water molecules where periodic boundary condition was applied. CHARMM all atom force field [44, 45] (version c35b2) was employed for $A\beta_{25-35}/\alpha 7$ -nAChR complex, while the water was described by TIP3P model [46]. The long range Coulomb interactions were calculated by using the Particle-Mesh Ewald (PME) summation, and the non-bonded cutoff was set to 12 \AA to avoid the interactions with the self-images.

The complex and surrounding water molecules have first undergone an energy minimization process by using conjugate gradient minimization method at $T=0 \text{ K}$ to reconcile the molecule structure and avoid the conformation with high potential energy. Then the system temperature was raised to room temperature (298 K) by a heating process. MD simulation was carried out by using Langevin-piston Nosé-Hoover method at 298 K



Scheme 1. Illustration of amide-I_a and amide-I_b vibrational modes in polypeptides. For color image, see the online version.

for 2 ns at the time step of 1 fs under NPT ensemble. The binding free energy of $A\beta_{25-35}/\alpha 7$ -nAChR complex (ΔG_{bind}) was calculated using the molecular mechanics Poisson-Boltzmann surface area (MM/PBSA) approach [47], and cluster analysis was applied on the all atom MD trajectory using a root mean square deviation (RMSD) tolerance of 1.5 \AA for the most representative clusters with the help of AMBER package [48].

C. Mapping the amide-I band of $A\beta_{25-35}$

The amide-I vibration is known to be sensitive to the secondary structure of polypeptides (Scheme 1). Here, the amide-I band was simulated for the $A\beta_{25-35}$ fragment within the complex in aqueous solution by using the electrostatic frequency map [38]. The electrostatic potentials from water, receptor, backbone and side chain of $A\beta_{25-35}$ were calculated and projected onto the atomic sites of amide units of $A\beta_{25-35}$. The conformational dependent amide-I frequency database obtained from DFT calculation was introduced for the snapshots throughout the MD trajectory.

The amide-I band trajectory can be obtained after applying the parameters of amide-I vibrational map constructed in our previous work to the MD trajectory of the docking complex by using the following equations [38, 49],

$$v_N = v_0 + \sum_{i=1}^4 f_i \varphi_i + f_5 \Delta v_{b,(\Phi, \Psi)} \quad (1)$$

$$v_N = v_0 + \frac{1}{2} \left[\left(\sum_{i=1}^4 f_i \varphi_i + f_5 \Delta v_{b,(\Phi, \Psi)} \right)_{R_n} + \left(\sum_{i=1}^4 f_i \varphi_i + f_5 \Delta v_{a,(\Phi, \Psi)} \right)_{R_{n+1}} \right] \quad (2)$$

Here, v_N is the amide-I frequency of the N th amide unit, v_0 is the experimental measured amide-I frequency of NMA in gas phase [50], φ is electrostatic potential on the amide unit (namely C, O, N, and H atoms), f_i is map parameters obtained from our previous work [38], Δv_a and Δv_b are the frequency differences from

the amide-I_a and amide-I_b modes assigned as the DFT calculated frequencies of dipeptides' conformers against ν_0 , R_n is the residue number for the selection of corresponding map parameters. The amide-I frequencies of amide units at C- and N-terminals were calculated by using Eq.(3), while the amide-I frequency of the N th ($N=2-9$) amide unit within the backbone was calculated according to Eq.(4). The possible vibrational couplings between the neighboring amide groups and nearby side chains were taken into account for the prediction of amide-I band of $A\beta_{25-35}$.

D. Virtual screening

Molecular docking method was employed for the screening of the lead compounds with activity on the $\alpha 7$ -nAChR in ZINC, NCBI, and IBS databases. The training set of these screened lead compounds was established for pharmacophore simulation to identify the necessary functional groups, then the new inhibitor was designed according to the rearrangement of these functional groups.

Structural optimization and normal mode analysis were performed for the designed drugs at B3LYP/6-31+G(d) level of theory by using Gaussian 09 software [51]. The vibrational motions reflected in the simulated IR spectra were assigned according to the potential energy distribution [52]. Semi-flexible docking method was employed for the demonstration of binding mechanism between the new drugs and $\alpha 7$ -nAChR. The binding competition between new drugs and $A\beta_{25-35}$ within the ion channel of receptor is then revealed for the evaluation of the potential usage of new drugs for AD treatment.

III. RESULTS AND DISCUSSION

A. Molecular docking of $A\beta_{25-35}$ and $\alpha 7$ -nAChR

Semi-flexible docking was used to understand the interactions between $A\beta_{25-35}$ and $\alpha 7$ -nAChR. Although total 31 pockets were found within $\alpha 7$ -nAChR, the $A\beta_{25-35}$ fragment can only bind to the 5th pocket of receptor. The favorable binding pose of $A\beta_{25-35}$ to the receptor's pocket (with its docking score of 58.81) was selected to elucidate the interaction between the ligand and receptor. The binding site is located near the N-terminal of two $\alpha 7$ subunit of receptor, and the $A\beta_{25-35}$ is just inserted into the ion channel of $\alpha 7$ -nAChR (FIG. 2(A)).

$A\beta_{25-35}$ tends to enter the ion channel of $\alpha 7$ -nAChR and binds to the surrounding residues with non-bonded interactions (FIG. 2(B)). The O-H group of Ser26 in $A\beta_{25-35}$ forms strong H-bond (1.4 Å) with C=O group of Val85 in E-chain of receptor, and a 1.9 Å H-bond is found between N-H group in the N-terminal of $A\beta_{25-35}$

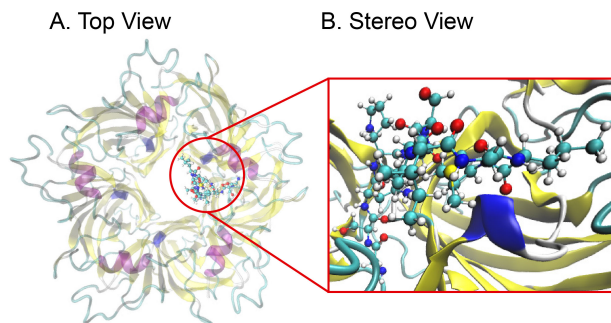


FIG. 2 The most preferred conformation of $A\beta_{25-35}/\alpha 7$ -nAChR complex and their binding interface. (A) Top view and (B) stereo view. For color image, see the online version.

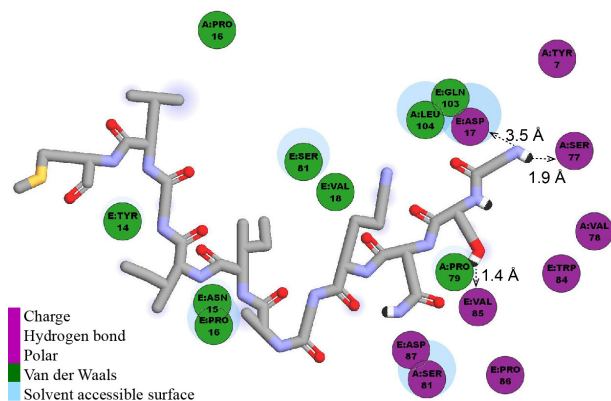


FIG. 3 The schematic diagram of the interactions between $A\beta_{25-35}$ and $\alpha 7$ -nAChR (hydrogen bonds are denoted as arrows). For color image, see the online version.

and Ser77 in A-chain of receptor, and a relatively weak H-bond (3.5 Å) is also formed between N-H group in the N-terminal of $A\beta_{25-35}$ and Asp17 in E-chain of receptor (FIG. 3). Therefore, with the help of H-bond together with the charge-charge interactions and the van der Waals forces and *etc.*, $A\beta_{25-35}$ binds to $\alpha 7$ -nAChR and forms stable complex.

For the evaluation of the aggregation process of $A\beta_{25-35}$ in the ion channel of $\alpha 7$ -nAChR, the docking complex was treated as a new receptor, and the active pocket was found for further docking of $A\beta_{25-35}$ into the ion channel. The obtained maximum docking score is 92.76, indicating that non-bonded interactions among two $A\beta_{25-35}$ and receptor are much stronger than the result obtained from one $A\beta_{25-35}$ and receptor after the second $A\beta_{25-35}$ enter the ion channel of receptor. The second $A\beta_{25-35}$ tends to form dimer with the first $A\beta_{25-35}$ through hydrogen bond, therefore, their binding site also locates near the N-terminal of two $\alpha 7$ subunit of receptor (FIG. 4), and the non-bonded interactions between second $A\beta_{25-35}$ and receptor is non-negligible.

Strong hydrogen bonds are formed between amide groups of ligand $A\beta_{25-35}$ and ASP27 of $A\beta_{25-35}$ in the

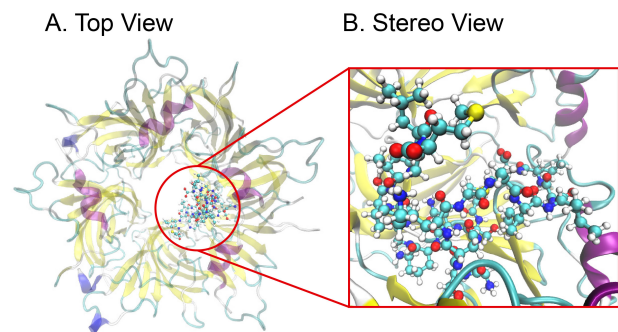


FIG. 4 The most preferred conformation of $2A\beta_{25-35}/\alpha 7$ -nAChR complex and their binding interface ((A) top view and (B) stereo view). For color image, see the online version.

complex with their lengths of 1.1 Å and 2.2 Å, respectively. Hydrogen bond is also observed between the side chain of ligand $A\beta_{25-35}$ and $A\beta_{25-35}$ (MET35) in the complex with the length of 2.4 Å, and the ligand $A\beta_{25-35}$ forms strong hydrogen bond (1.7 Å) with SER47 of A-chain (FIG. 5). The obtained results clearly revealed that the ligand $A\beta_{25-35}$ enters the ion channel and binds to the complex via non-bonded interactions such as hydrogen bond and the complementary shape.

The ion channel of $\alpha 7$ -nAChR receptor is jammed after two $A\beta_{25-35}$ fragments enter it. No more $A\beta_{25-35}$ fragment would enter the ion channel due to the steric hindrance effect. The transportation of Ca^{2+} through the ion channel is blocked at the same time, leads to the Ca^{2+} regulation imbalance and the malfunction of synapsis, and thus induces the AD.

B. Structural dynamics of $A\beta_{25-35}/\alpha 7$ -nAChR complex

The energy and RMSD of $A\beta_{25-35}/\alpha 7$ -nAChR complex in aqueous solution throughout the MD trajectory is shown in FIG. 6. It is shown that the complex system is stabilized after 0.5 ns, the RMSD ranges from 0.981 Å to 1.441 Å during 0.5–2 ns with its average value of 1.213 Å, and the energy mostly fluctuates from around -2.50×10^5 kcal/mol to -2.47×10^5 kcal/mol. $A\beta_{25-35}$ binds to receptor with strong non-bonded interactions and the whole system is quite stable. The total binding free energy of the complex is -53.4 kcal/mol obtained by using MM-PBSA method, indicating that $A\beta_{25-35}$ tends to enter the ion channel of receptor and form a stable complex.

Cluster analysis was performed for the all atom MD trajectory of $A\beta_{25-35}$ fragment, and the most representative clusters were obtained by using the `g_cluster` module in Gromacs package [53], and visualized in VMD software [54]. The two most representative clusters of $A\beta_{25-35}$ within the docking complex in aqueous solution are shown in FIG. 7. $A\beta_{25-35}$ mainly presents random coil structure at 298 K with the cutoff of RMSD

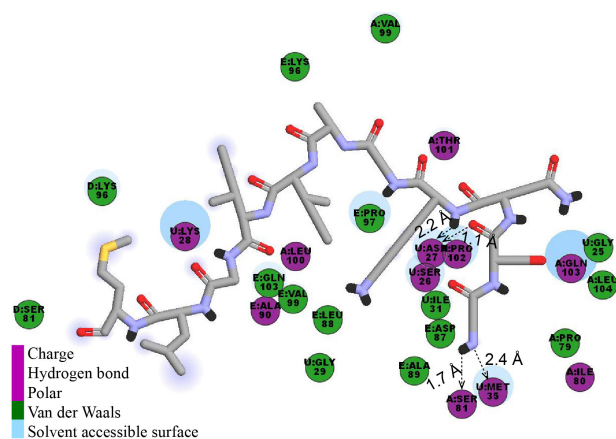


FIG. 5 The schematic diagram of the interactions between $A\beta_{25-35}$ and $A\beta_{25-35}/\alpha 7$ -nAChR complex (hydrogen bonds are denoted as arrows). For color image, see the online version.

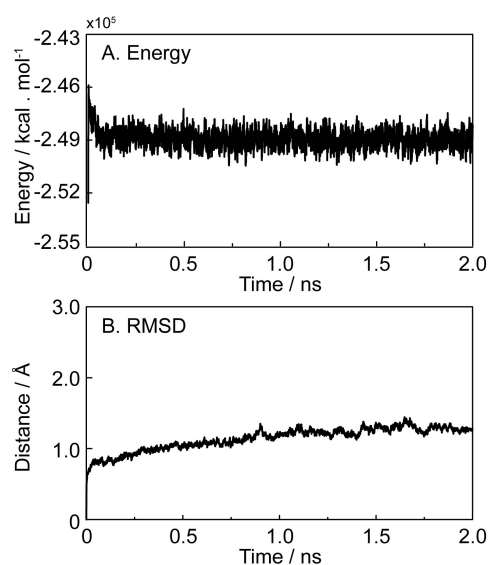


FIG. 6 The energy fluctuation (A) and RMSD (B) of the $A\beta_{25-35}/\alpha 7$ -nAChR complex during MD simulation.

set to 0.3 nm. The main difference between cluster 1 (89.12%) and cluster 2 (10.88%) is the folding directions of ILE31 and ILE32.

For the understanding of the aggregation mechanism of $A\beta_{25-35}$ fragments within the $\alpha 7$ -nAChR, 2 ns MD simulation was performed for the docked complex consisting of two $A\beta_{25-35}$ fragments and $\alpha 7$ -nAChR, the most preferred docking pose was set for the initial conformation. The total energy and calculated RMSD of MD trajectory show that the system is stable after 0.5 ns production run (FIG. 8).

The RMSD is calculated based on the $2A\beta_{25-35}/\alpha 7$ -nAChR complex system which consists of 16765 atoms. The RMSD value ranges from 1.291 Å to 1.799 Å during 0.5–2 ns with its average value of 1.456 Å. The RMSD is quite small and stable considering the size of the

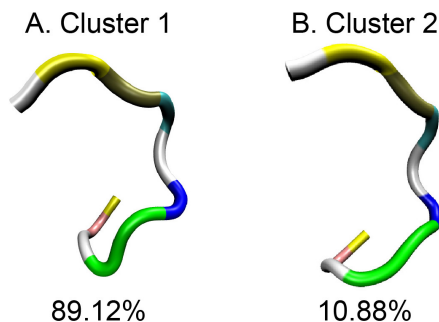


FIG. 7 The most representative clusters of $A\beta_{25-35}$ in $A\beta_{25-35}/\alpha 7$ -nAChR complex. For color image, see the online version.

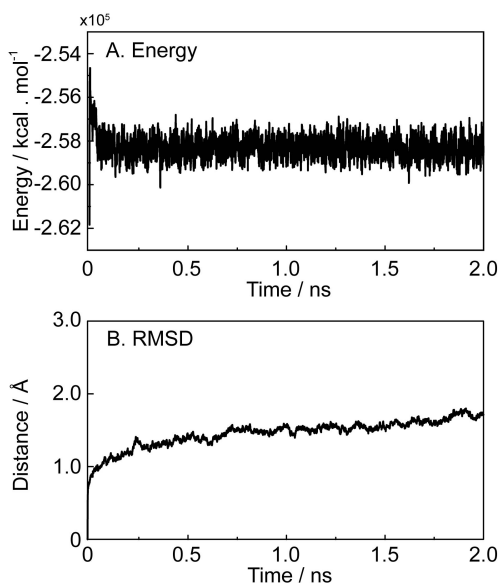


FIG. 8 The energy fluctuation (A) and RMSD (B) of $2A\beta_{25-35}/\alpha 7$ -nAChR complex during MD simulation.

complex system, and the energy mostly fluctuates from around -2.60×10^5 kcal/mol to -2.57×10^5 kcal/mol, indicating that the complex is quite stable after the two $A\beta$ fragments enter the ion channel of receptor. Therefore, the sampled MD trajectory is representative enough for the structural fluctuation of the complex system.

MM-PBSA result shows that the binding energy is -28.8 kcal/mol, indicating that the second $A\beta_{25-35}$ can easily enter the ion channel and the whole system tends to be stable. There are strong intermolecular interactions between two $A\beta_{25-35}$ fragments, and they tend to form stable $A\beta_{25-35}$ dimer within the receptor, therefore the ion channel is then blocked.

Molecular docking was performed to reveal the maximum capacity of $A\beta$ fragment (two $A\beta_{25-35}$) within the ion channel of the receptor, then the MD simulations were carried out for the demonstration of the structural preference and the stability of $2A\beta_{25-35}/\alpha 7$ -nAChR complex. The results show that strong non-

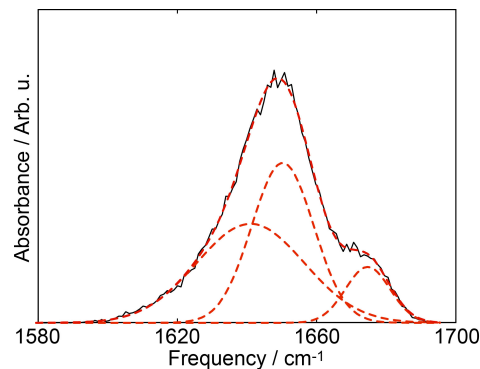


FIG. 9 The static frequency distribution and its Gaussian fitting for the amide-I band of $A\beta_{25-35}$ fragment within complex in aqueous solution. For color image, see the online version.

bond interactions can be found among three molecules (FIG. 5). Since the energy becomes stable soon in the MD production run (FIG. 8(A)), it is assumed that three molecules rapidly adjust their conformations to make sure the complex system is stable. Therefore, no matter whether the two $A\beta$ fragments first combine with each other or they enter the ion channel one by one, they will finally reach the same conformational basin that forms a stable $2A\beta_{25-35}/\alpha 7$ -nAChR complex system.

C. Amide-I band of $A\beta_{25-35}$

The amide-I band of $A\beta_{25-35}$ within the receptor in aqueous solution is simulated by using the map protocol. The electrostatic potentials that projected on the amide atomic sites were calculated for all the instantaneous structures throughout the MD trajectory. The location of the amide-I band is mostly contributed by the electrostatic potentials originated from the receptor, surrounding solvent, backbone and side chain of $A\beta_{25-35}$, and the secondary structural dependent amide-I frequencies databases were introduced for the amide-I band prediction [38]. The static frequency distribution of amide-I band is obtained after applying the map coefficients of recently built hybrid map with general application for polypeptides and proteins [38] to the electrostatic potentials on the backbone amide units of $A\beta_{25-35}$ (FIG. 9).

The amide-I band can be fitted with Gaussian function, and the fitting result consists of three peaks located at 1641.1 cm^{-1} , 1650.5 cm^{-1} , and 1675.1 cm^{-1} , indicating $A\beta_{25-35}$ tends to form random coil and turn structure. The most probable distributed amide-I peak at 1650.5 cm^{-1} shows that $A\beta_{25-35}$ mainly presents random coil conformation, which is consistent with the results from cluster analysis. The interpretation of the amide-I band has the potentials in understanding the molecular structure and dynamics of polypeptides in

aqueous solution.

D. Virtual screening targeted on $\alpha 7$ -nAChR

The above analysis has shown that $A\beta_{25-35}$ fragments can easily enter the ion channel of $\alpha 7$ -nAChR, and form stable oligomer. To inhibit or slow down the aggregation of $A\beta_{25-35}$ fragments in the ion channel, effective inhibitor should be screened for better AD treatment based on the existing drugs.

Here, virtual screening was carried out for the existing drugs that can dock to the active pocket of $\alpha 7$ -nAChR from ZINC, NCBI, and IBS databases. The results show that only six drug molecules from ZINC database can bind to the active pockets that $A\beta_{25-35}$ prefers to dock within the ion channel of $\alpha 7$ -nAChR (FIG. 10). The official numbers of these drugs in ZINC database are 49942739, 49592897, 28861883, 45374657, 28861885, and 49946824, respectively, and the docking score of the most preferred docking poses of these drugs docking to $\alpha 7$ -nAChR are 56.95, 67.37, 69.98, 75.16, 85.31, and 89.04, respectively.

There are five screened drugs which have higher docking score than $A\beta_{25-35}$ when they bind to $\alpha 7$ -nAChR, while the other one drug has similar docking score. However, all the six screened drugs have lower docking score compared with two $A\beta_{25-35}$ fragments bind to the ion channel of receptor. Therefore, these drugs might have the potential of inhibiting the entry of $A\beta_{25-35}$ into the ion channel of $\alpha 7$ -nAChR at the early stage of AD, but still have difficulty in the treatment of AD.

E. Drug design and docking with $\alpha 7$ -nAChR

The above six drugs were set as lead compounds for pharmacophore simulation. The hydrophobic centers of these lead compounds are mostly aromatic ring and alkane. To obtain new drugs, the lead compounds are split into different side chains and groups, then these functional groups are rearranged into eight new drugs named as h1 to h8 (FIG. 11). According to the molecular symmetry, h1 to h4 can be classified into one category while h5 to h8 into another.

Semi-flexible docking was applied for the eight new drugs binding to $\alpha 7$ -nAChR. The docking results show that there are strong inter-molecular interactions between these drugs in the active pockets of the receptor. The most preferred docking poses between these new drugs and $\alpha 7$ -nAChR are shown in FIG. 12, and the corresponding docking scores are 77.15, 109.42, 82.52, 54.65, 73.07, 80.07, 74.87, and 75.97, respectively. These designed new drugs tend to dock into the ion channel of $\alpha 7$ -nAChR, and possess higher docking scores compared with one $A\beta_{25-35}$, except for h4 whose docking score is relatively lower. Comparing with the lead compounds, the docking scores of these new

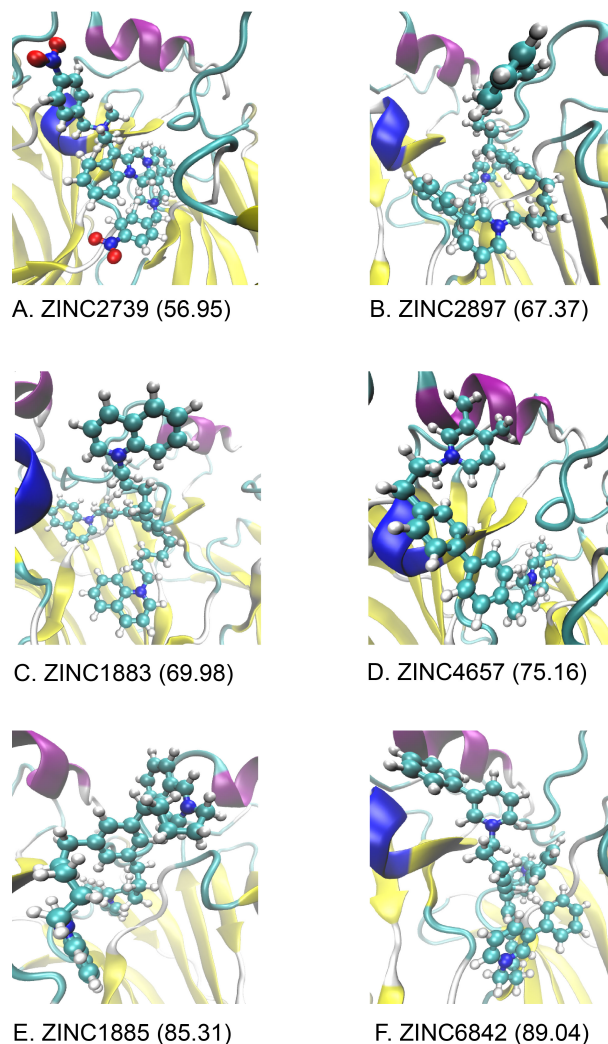


FIG. 10 The most preferred docking poses between screened drugs and $\alpha 7$ -nAChR. For color image, see the online version.

drugs are much higher, indicating that the new drugs have much stronger tendency binding to the $\alpha 7$ -nAChR, therefore, the new drugs have the potential of inhibiting the entry of $A\beta_{25-35}$ fragments into the ion channel.

These eight drugs strongly bind to receptor through geometry matching and non-bonded interactions. Conjugation effects like σ - π , π - π interactions between h1, h2, h7 and $\alpha 7$ -nAChR are found to be stronger than other drugs, while only π - π conjugation is observed for h5. These non-bonded interactions between new drugs and the receptor would stabilize their binding, and the entry of $A\beta_{25-35}$ fragment into the ion channel will be blocked due to the stronger affinity between the drug and $\alpha 7$ -nAChR, thus inhibiting the aggregation of $A\beta_{25-35}$ in the ion channel. The results indicate that the new drugs have the potential of slowing down the onset of AD except h4.

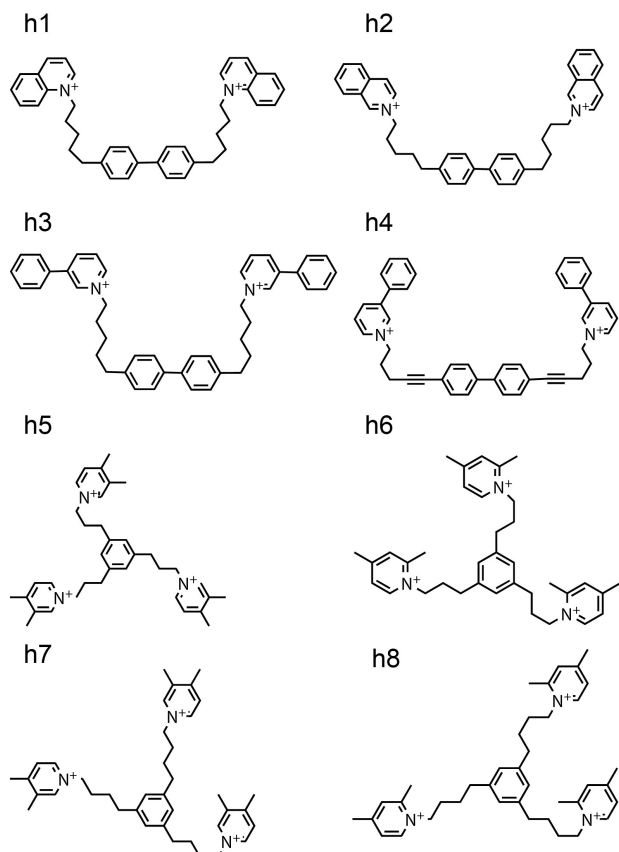
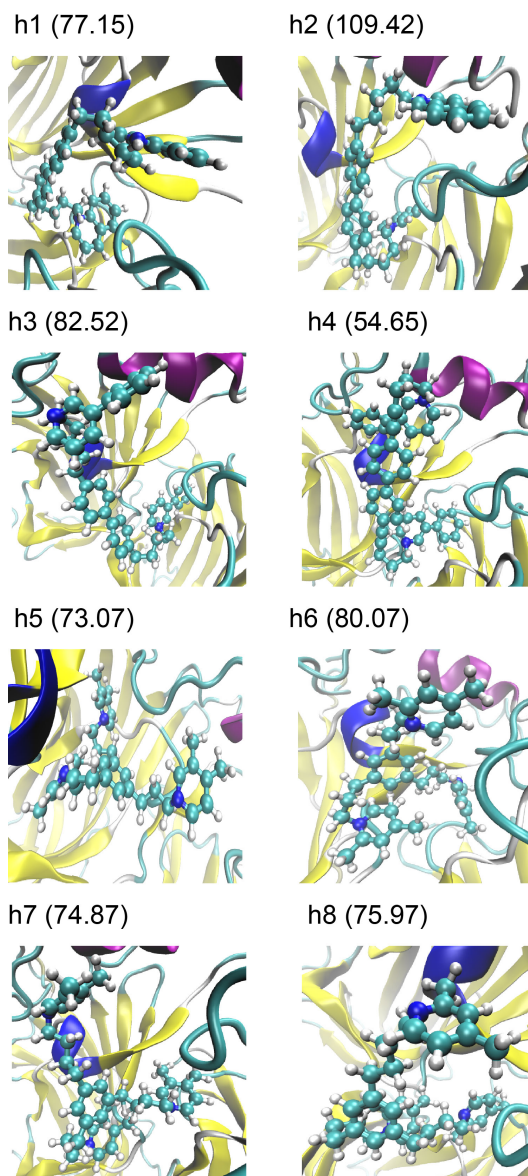


FIG. 11 Molecular structures of designed new drugs.

IV. CONCLUSION

Molecular docking, molecular dynamics simulations, spectral modeling and virtual screening methods were employed for the understanding about the interactions between $A\beta_{25-35}$ and $\alpha 7$ -nAChR. Semi-flexible docking results show that $A\beta_{25-35}$ binds to the ion channel of $\alpha 7$ -nAChR through non-bonded interactions like hydrogen bond, π - π stacking, and van der Waals force. $A\beta_{25-35}$ fragments tend to aggregate in the ion channel of $\alpha 7$ -nAChR, where strong affinity can also be found between $A\beta_{25-35}$ fragments. MD simulations show that the docking complex of $A\beta_{25-35}/\alpha 7$ -nAChR is quite stable, and the $A\beta_{25-35}$ fragment stays in the ion channel of receptor and blocks the ion transportation. The predicted amide-I band shows that $A\beta_{25-35}$ mainly presents random coil conformation which is consistent with the results from cluster analysis.

Virtual screening was performed to obtain six existing drugs as lead compounds that can dock to the active pocket of $\alpha 7$ -nAChR, and then eight new drugs were obtained after the pharmacophore simulation. These new drugs can strongly dock to the receptor with non-bonded interactions, and have the power of inhibiting the binding and aggregation of $A\beta_{25-35}$ fragments in the ion channel of receptor. These results bring us new

FIG. 12 The most preferred docking poses between new drugs and $\alpha 7$ -nAChR. For color image, see the online version.

insight into the interactions between $A\beta_{25-35}$ and $\alpha 7$ -nAChR at atomic level, which would be helpful for our understanding about the onset of AD, and also provide theoretical support for the new drug development.

V. ACKNOWLEDGMENTS

This work was supported by the National Natural Science Foundation of China (No.21103021), the New Century Excellent Talent Project in University of Fujian Province, Opening Project of PCOSS, Xiamen University (No.201904).

- [1] X. Zhou, Y. Chen, K. Y. Mok, Q. Zhao, K. Chen, Y. Chen, J. Hardy, Y. Li, A. K. Y. Fu, Q. Guo, N. Y. Ip, and N. I. Alzheimer's Dis, *Proc. Natl. Acad. Sci. USA* **115**, 1697 (2018).
- [2] M. Lorenzi, A. Altmann, B. Gutman, S. Wray, C. Arber, D. P. Hibar, N. Jahanshad, J. M. Schott, D. C. Alexander, P. M. Thompson, S. Ourselin, and N. Alzheimer's Dis, *Proc. Natl. Acad. Sci. USA* **115**, 3162 (2018).
- [3] D. D. Chu and F. Liu, *ACS Chem. Neurosci.* **10**, 931 (2019).
- [4] C. M. Dobson, *Trends Biochem. Sci.* **24**, 329 (1999).
- [5] C. M. Dobson, *Nature* **426**, 884 (2003).
- [6] M. Stefani and C. M. Dobson, *J. Mol. Med.* **81**, 678 (2003).
- [7] A. S. DeToma, S. Salamekh, A. Ramamoorthy, and M. H. Lim, *Chem. Soc. Rev.* **41**, 608 (2012).
- [8] S. Parthasarathy, M. Inoue, Y. Xiao, Y. Matsumura, Y. I. Nabeshima, M. Hoshi, and Y. Ishii, *J. Am. Chem. Soc.* **137**, 6480 (2015).
- [9] A. S. Y. Law, L. C. C. Lee, M. C. L. Yeung, K. K. W. Lo, and V. W. W. Yam, *J. Am. Chem. Soc.* **141**, 18570 (2019).
- [10] I. W. Hamley, *Angew. Chem. Int. Edit.* **46**, 8128 (2007).
- [11] K. Kurbatskaya, E. C. Phillips, C. L. Croft, G. Dentoni, M. M. Hughes, M. A. Wade, S. Al-Sarraj, C. Troakes, M. J. O'Neill, B. G. Perez-Nievas, D. P. Hanger, and W. Noble, *Acta Neuropathol. Commun.* **4**, 34 (2016).
- [12] C. M. Henstridge, E. Pickett, and T. L. Spires-Jones, *Ageing Res. Rev.* **28**, 72 (2016).
- [13] C. Wallin, Y. Hiruma, S. K. T. S. Wärmländer, I. Huvent, J. Jarvet, J. P. Abrahams, A. Gräslund, G. Lip-pens, and J. Luo, *J. Am. Chem. Soc.* **140**, 8138 (2018).
- [14] N. J. Economou, M. J. Giammona, T. D. Do, X. Zheng, D. B. Teplow, S. K. Buratto, and M. T. Bowers, *J. Am. Chem. Soc.* **138**, 1772 (2016).
- [15] B. Murray, B. Sharma, and G. Belfort, *ACS Chem. Neurosci.* **8**, 432 (2017).
- [16] C. J. Pike, A. J. Walencewicz-Wasserman, J. Kosmoski, D. H. Cribbs, C. G. Glabe, and C. W. Cotman, *J. Neurochem.* **64**, 253 (1995).
- [17] A. M. D'Ursi, M. R. Armenante, R. Guerrini, S. Salvadori, G. Sorrentino, and D. Picone, *J. Med. Chem.* **47**, 4231 (2004).
- [18] E. Terzi, G. Hoelzemann, and J. Seelig, *Biochemistry* **33**, 7434 (1994).
- [19] T. Kohno, K. Kobayashi, T. Maeda, K. Sato, and A. Takashima, *Biochemistry* **35**, 16094 (1996).
- [20] M. del Mar Martínez-Senac, J. Villalaín, and J. C. Gómez-Fernández, *Eur. J. Biochem.* **265**, 744 (1999).
- [21] Q. S. Liu, H. Kawai, and D. K. Berg, *Proc. Natl. Acad. Sci. USA* **98**, 4734 (2001).
- [22] D. Bertrand, J. L. Galzi, A. Devillers-Thiéry, S. Bertrand, and J. P. Changeux, *Proc. Natl. Acad. Sci.* **90**, 6971 (1993).
- [23] K. T. Dineley, A. A. Pandya, and J. L. Yakel, *Trends Pharmacol. Sci.* **36**, 96 (2015).
- [24] H. Lin, S. Vicini, F. C. Hsu, S. Doshi, H. Takano, D. A. Coulter, and D. R. Lynch, *Proc. Natl. Acad. Sci. USA* **107**, 16661 (2010).
- [25] L. A. Mohamed, H. Qosa, and A. Kaddoumi, *ACS Chem. Neurosci.* **6**, 725 (2015).
- [26] M. Criado, J. Mulet, F. Sala, S. Sala, I. Colmena, L. Gandia, O. M. Bautista-Aguilera, A. Samadi, M. Chioua, and J. Marco-Contelles, *ACS Chem. Neurosci.* **7**, 1157 (2016).
- [27] A. K. Hamouda, T. Kimm, and J. B. Cohen, *J. Neurosci.* **33**, 485 (2013).
- [28] W. Qiang, W. M. Yau, J. X. Lu, J. Collinge, and R. Tycko, *Nature* **541**, 217 (2017).
- [29] S. D. Moran and M. T. Zanni, *J Phys. Chem. L* **5**, 1984 (2014).
- [30] A. M. Alperstein, J. S. Ostrander, T. O. Zhang, and M. T. Zanni, *Proc. Natl. Acad. Sci. USA* 201821534 (2019).
- [31] M. K. Petti, J. P. Lomont, M. Maj, and M. T. Zanni, *J. Phys. Chem. B* **122**, 1771 (2018).
- [32] M. C. Asplund, M. T. Zanni, and R. M. Hochstrasser, *Proc. Natl. Acad. Sci. USA* **97**, 8219 (2000).
- [33] A. Remorino and R. M. Hochstrasser, *Acc. Chem. Res.* **45**, 1896 (2012).
- [34] C. R. Baiz, B. Błasiak, J. Bredenbeck, M. Cho, J. H. Choi, S. A. Corcelli, A. G. Dijkstra, C. J. Feng, S. Garrett-Roe, N. H. Ge, M. W. D. Hanson-Heine, J. D. Hirst, T. L. C. Jansen, K. Kwac, K. J. Kubarych, C. H. Londergan, H. Maekawa, M. Reppert, S. Saito, S. Roy, J. L. Skinner, G. Stock, J. E. Straub, M. C. Thielges, K. Tominaga, A. Tokmakoff, H. Torii, L. Wang, L. J. Webb, and M. T. Zanni, *Chem. Rev.* **120**, 7152 (2020).
- [35] K. Cai, T. Su, S. Lin, and R. Zheng, *Spectrochim. Acta Part A* **117**, 548 (2014).
- [36] K. Cai, F. Du, X. Zheng, J. Liu, R. Zheng, J. Zhao, and J. Wang, *J. Phys. Chem. B* **120**, 1069 (2016).
- [37] K. Cai, X. Zheng, and F. Du, *Spectrochim. Acta, Part A* **183**, 150 (2017).
- [38] K. Cai, X. Zheng, J. Liu, F. Du, G. Yan, D. Zhuang, and S. Yan, *Spectrochim. Acta Part A* **219**, 391 (2019).
- [39] J. K. Carr, A. V. Zabuga, S. Roy, T. R. Rizzo, and J. L. Skinner, *J. Chem. Phys.* **140**, 224111 (2014).
- [40] C. J. Feng and A. Tokmakoff, *J. Chem. Phys.* **147**, 085101 (2017).
- [41] A. Ghosh, J. S. Ostrander, and M. T. Zanni, *Chem. Rev.* **117**, 10726 (2017).
- [42] M. Reppert and A. Tokmakoff, *Annu. Rev. Phys. Chem.* **67**, 359 (2016).
- [43] J. C. Phillips, R. Braun, W. Wang, J. Gumbart, E. Tajkhorshid, E. Villa, C. Chipot, R. D. Skeel, L. Kale, and S. Klaus, *J. Comput. Chem.* **26**, 1781 (2005).
- [44] A. D. MacKerell Jr., D. Bashford, M. Bellott, R. L. Dunbrack Jr., J. D. Evanseck, M. J. Field, S. Fischer, J. Gao, H. Guo, S. Ha, D. Joseph-McCarthy, L. Kuchnir, K. Kuczera, F. T. K. Lau, C. Mattos, S. Michnick, T. Ngo, D. T. Nguyen, B. Prodhom, W. E. Reiher III, B. Roux, M. Schlenkrich, J. C. Smith, R. Stote, J. Straub, M. Watanabe, J. Wiorkiewicz-Kuczera, D. Yin, and M. Karplus, *J. Phys. Chem. B* **102**, 3586 (1998).
- [45] A. D. MacKerell Jr., M. Feig, and C. L. Brooks, *J. Comput. Chem.* **25**, 1400 (2004).
- [46] W. L. Jorgensen, J. Chandrasekhar, J. D. Madura, R. W. Impey, and M. L. Klein, *J. Chem. Phys.* **79**, 926 (1983).
- [47] B. R. Miller, T. D. McGee, J. M. Swails, N. Homeyer, H. Gohlke, and A. E. Roitberg, *J. Chem. Theory Comput.* **8**, 3314 (2012).
- [48] D. A. Case, T. E. Cheatham, T. Darden, H. Gohlke,

- R. Luo, K. M. Merz, A. Onufriev, C. Simmerling, B. Wang, and R. J. Woods, *J. Comput. Chem.* **26**, 1668 (2005).
- [49] K. Cai, X. Zheng, Y. Liu, S. Liu, and F. Du, *Acta Phys. Chim. Sin.* **32**, 1289 (2016).
- [50] L. C. Mayne and B. Hudson, *J. Phys. Chem.* **95**, 2962 (1991).
- [51] M. J. Frisch, G. W. Trucks, H. B. Schlegel, G. E. Scuseria, M. A. Robb, J. R. Cheeseman, G. Scalmani, V. Barone, B. Mennucci, G. A. Petersson, H. Nakatsuji, M. Caricato, X. Li, H. P. Hratchian, A. F. Izmaylov, J. Bloino, G. Zheng, J. L. Sonnenberg, M. Hada, M. Ehara, K. Toyota, R. Fukuda, J. Hasegawa, M. Ishida, T. Nakajima, Y. Honda, O. Kitao, H. Nakai, T. Vreven, J. Montgomery, J. A. , J. E. Peralta, F. Ogliaro, M. Bearpark, J. J. Heyd, E. Brothers, K. N. Kudin, V. N. Staroverov, R. Kobayashi, J. Normand, K. Raghavachari, A. Rendell, J. C. Burant, S. S. Iyengar, J. Tomasi, M. Cossi, N. Rega, N. J. Millam, M. Klene, J. E. Knox, J. B. Cross, V. Bakken, C. Adamo, J. Jaramillo, R. Gomperts, R. E. Stratmann, O. Yazyev, A. J. Austin, R. Cammi, C. Pomelli, J. W. Ochterski, R. L. Martin, K. Morokuma, V. G. Zakrzewski, G. A. Voth, P. Salvador, J. J. Dannenberg, S. Dapprich, A. D. Daniels, Ö. Farkas, J. B. Foresman, J. V. Ortiz, J. Cioslowski, and D. J. Fox, *Gaussian 09, Revision A.01*, Wallingford CT.: Gaussian Inc., (2009).
- [52] M. H. Jamroz, *Spectrochim. Acta Part A* **114**, 220 (2013).
- [53] S. Pronk, S. Pall, R. Schulz, P. Larsson, P. Bjelkmar, R. Apostolov, M. R. Shirts, J. C. Smith, P. M. Kasson, D. van der Spoel, B. Hess, and E. Lindahl, *Bioinformatics* **29**, 845 (2013).
- [54] W. Humphrey, A. Dalke, and K. Schulten, *J. Mol. Graphics* **14**, 33 (1996).